

Supporting Information for

Insights into Endosomal Escape Mechanism via Investigation of Dendrimer-Membrane Interactions

Wen-de Tian[†] and Yu-qiang Ma^{††*}

Model and Methods

The MARTINI coarse-grained (CG) force field developed by Marrink et al.¹ was employed to model all species for the systems under investigation. The MARTINI model maps every four heavy atoms (i.e., not hydrogen atoms) into one effective particle. Each of these particles is assigned a diameter $\sigma = 0.47$ nm. Van der Waals interactions are modeled using the Lennard-Jones(LJ) 12-6 potential. There are four main types of effective particles representing different levels of interaction: polar (P), apolar (C), nonpolar (N), and charged (Q). Ten different levels of interaction exist to differentiate between various particle types. Covalent bonds between CG particles are described by harmonic spring potentials. Angular potentials are modeled with a harmonic cosine potential. The MARTINI force field has been used for lipids, water, ions, protein, and dendrimers.¹⁻³

The mapping of the dipalmitoyl phosphatidylcholine (DPPC), dipalmitoyl phosphatidylethanolamine (DPPE), and dipalmitoyl phosphatidylserine (DPPS) lipids used in our simulations into the coarse-grained beads in the framework of MARTINI force field² was shown in Figure S1 (a). The CG force field of these lipids and their topologies were downloaded from <http://md.chem.rug.nl/cgmartini/>. We construct two symmetrical bilayers (S1) with charge-neutral lipids of DPPC or DPPE, two negatively charged, symmetric bilayers (S2) through the replacement of DPPC or DPPE by DPPS, and three asymmetric bilayers (S3), the bottom leaflets of which are electronegative (see Table 1 in the text). Particularly, the asymmetric bilayer, S33, was built on the basis of the main lipid composition of plasma membrane of eukaryotic cell without cholesterol, sphingolipid, and proteins.⁴ Each lipid bilayer consists of 1000 lipid molecules with the composition shown in Table 1 in the text, surrounded by more than 60922 CG water particles (corresponding to 243688 water molecules). Construction of the lipid bilayer consists of the following steps: A preassembled DPPC lipid bilayer configuration with 250 lipids, equilibrated for 1 μ s, then it was replicated across the X and Y directions. According to our design of lipid composition in each system, the DPPC lipids were replaced by DPPE or DPPS lipids, and the counterions were added to keep the electro-neutral systems. Consequently, we obtained the initial conformation of seven lipid systems. Each system was then equilibrated for 500 ns in NPT ensemble to allow for a tensionless membrane to prepare further simulations. The final configuration of tensionless membrane of S33 system with the area per lipid 0.58 nm² was presented in Figure

S1 (b). To prepare the tense membrane, we applied a tension to stretch the membranes until the area per lipid reached the value we needed. Then the system was equilibrated for 500 ns in the NVT ensemble to produce the initial conformation of membrane under tension. The final membrane configuration of the S33 system under tension with the area per lipid 1.13 nm^2 was presented in Figure S1 (c) which shows the integrality of lipid bilayers, implying that the tension studied is below the critical tension splitting the membrane.

The polyamidoamine (PAMAM) dendrimers have primary amine groups at each branch end and tertiary amine groups at each branching point.⁵ At physiological pH (~ 7), the terminal monomer is positively charged because all of the primary amines are protonated, and most of the tertiary amines are protonated at low pH (~ 5).⁶ To mimic the two pH conditions, the corresponding protonation levels of dendrimers are considered via modeling the branching beads with charges, similar to the atomistic simulation.⁷ Figure S2 (a) illustrates the mapping of the generation 2 (G2) PAMAM dendrimer into the CG beads in the framework of MARTINI force field.^{2,3} Figure S2 (b) and (c) shows the mapping of dendrimer chemical moieties and the topology of the G1 PAMAM dendrimer at physiological pH. The mapping of dendrimers in two pH states was also checked through comparing with atomistic simulations (Table S1). Similar to Lee et al.,³ we calculate the radii of gyration of dendrimer in the water solution and compare them with the results of atomistic simulations.^{7,8} We found that our coarse-grained simulations agree with the results from those atomic simulations, which supports the rationality of the coarse-grained force field of dendrimers.

Initial atomic coordinates of well-defined G4 PAMAM dendrimers without folding were generated with the Material Studio software package, followed by several steps of energy minimization. The atomic coordinates of the nitrogen atom in each moiety were used to specify the initial position of each CG bead. We performed $1 \mu\text{s}$ long molecular dynamics simulations of CG dendrimers in solution. The cubic box has a typical box size of $\sim 16 \text{ nm}$ under periodic boundary conditions along XYZ directions. The counterions, Cl^- , and water beads were added into the box. A time step of 25 fs was used, and the coordinates were saved every 50 ps for analysis. The equilibrated conformations of dendrimers were analyzed to determine their sizes and used as starting configurations for further simulations. The final conformation of G4 dendrimers at low pH was given in Figure S2 (d).

To obtain the equilibration of each dendrimer-membrane system, the equilibrated dendrimer was added to the bilayer systems obtained from previous equilibration runs. The

center of mass of each dendrimer was positioned a distance of about 4 nm above the center of the bilayer. Water molecules and counterions were added to achieve electroneutrality. The dendrimers and the bilayers were then harmonically constrained for 100 ns with a force constant of $1000 \text{ kJ mol}^{-1} \text{ nm}^{-2}$ to equilibrate water and ions. After the constraint run, the dendrimers and the bilayers were released to interact freely. The unrestrained equilibration runs were performed for $1 \mu\text{s}$ with a time step of 25 fs. The coordinates were saved every 50 ps for analysis. Note that because of the smoothing of the potentials in the CG model, diffusive motion is faster than that in atomistic simulations and so the effective time sampled using CG is 3-6 times greater than that in atomistic simulations,¹ and hence the effective time step is approximately 100 fs, which is 4 times longer than the actual simulation time step. All other times reported in this paper are effective times.

All simulations and analyzes were performed with the GROMACS 4.5.1 simulation package.⁹ The simulations were carried out under periodic boundary conditions at constant temperature and pressure except the systems of membrane under tension, where we turned off the pressure control. The temperature was kept constant for each group at 310 K using the Berendsen thermostat¹⁰ with a relaxation time of 1 ps. The pressure of the system was coupled and maintained at 1 bar using the Berendsen algorithm¹⁰ with a time constant of 5 ps. A cutoff of 1.2 nm was used for van der Waals interactions, and electrostatic interactions were modeled using a combination of particle mesh Ewald summation (PME).¹¹ With use of the standard shift function of GROMACS in which both the energy and force vanish at the cutoff distance, the LJ potential was smoothly shifted to zero between 0.9 and 1.2 nm to reduce the cutoff noise. Simulations were visualized using Visual Molecular Dynamics (VMD) package.¹²

Supporting Table

Table S1. Radii of gyration(R_g) of dendrimers in equilibrium under neutral and low pH conditions compared with atomistic simulations^a

Environment	Lee et al. ⁸	Maiti et al. ⁷	This work
Neutral pH	2.67 ± 0.02	1.70 ± 0.01	1.81 ± 0.01
Acidic pH	2.99 ± 0.01	1.90 ± 0.01	2.22 ± 0.01

^a Lee et al.⁸ carried out atomistic simulations of dendrimers without explicit water. The validity of the force field they used was checked through comparing with the system of G2 dendrimers with explicit water molecules. Maiti et al.⁷ carried out atomistic simulations of dendrimers in explicit water. Our coarse-grained simulations qualitatively agree with the results from those atomic simulations.

Supporting Figures

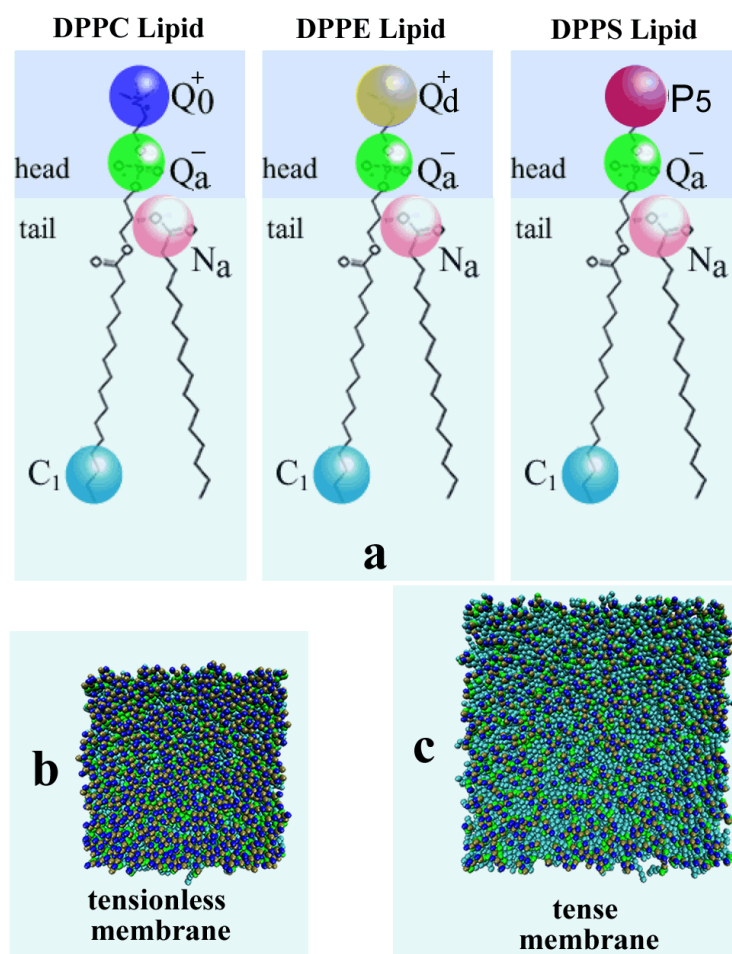


Figure S 1: (a) Mapping of the dipalmitoylphosphatidylcholine (DPPC), dipalmitoyl phosphatidylethanolamine (DPPE), and dipalmitoyl phosphatidylserine (DPPS) lipids into the coarse-grained beads in the framework of MARTINI force field.^{2,3} In the force field, there are mainly four types of interaction sites: polar (P), nonpolar (N), apolar (C), and charged (Q). Each type has a number of subtypes distinguished by a letter denoting the hydrogen-bonding capabilities (d = donor, a = acceptor, da = both, 0 = none), or by a number indicating the degree of polarity (from 1, low polarity, to 5, high polarity). (b) Top view of the final configuration of tensionless membrane of S33 systems with the area per lipid 0.58 nm^2 . (c) Top view of the final membrane configuration of the S33 system under tension with the area per lipid 1.13 nm^2 . The figure shows the integrality of lipid bilayers, implying that the tension studied is below the critical tension splitting the membrane. In (b) and (c), cyan beads represent tail groups of lipid bilayers, green and blue beads represent headgroups of the bilayers. Water and counterions are not shown for clarity.

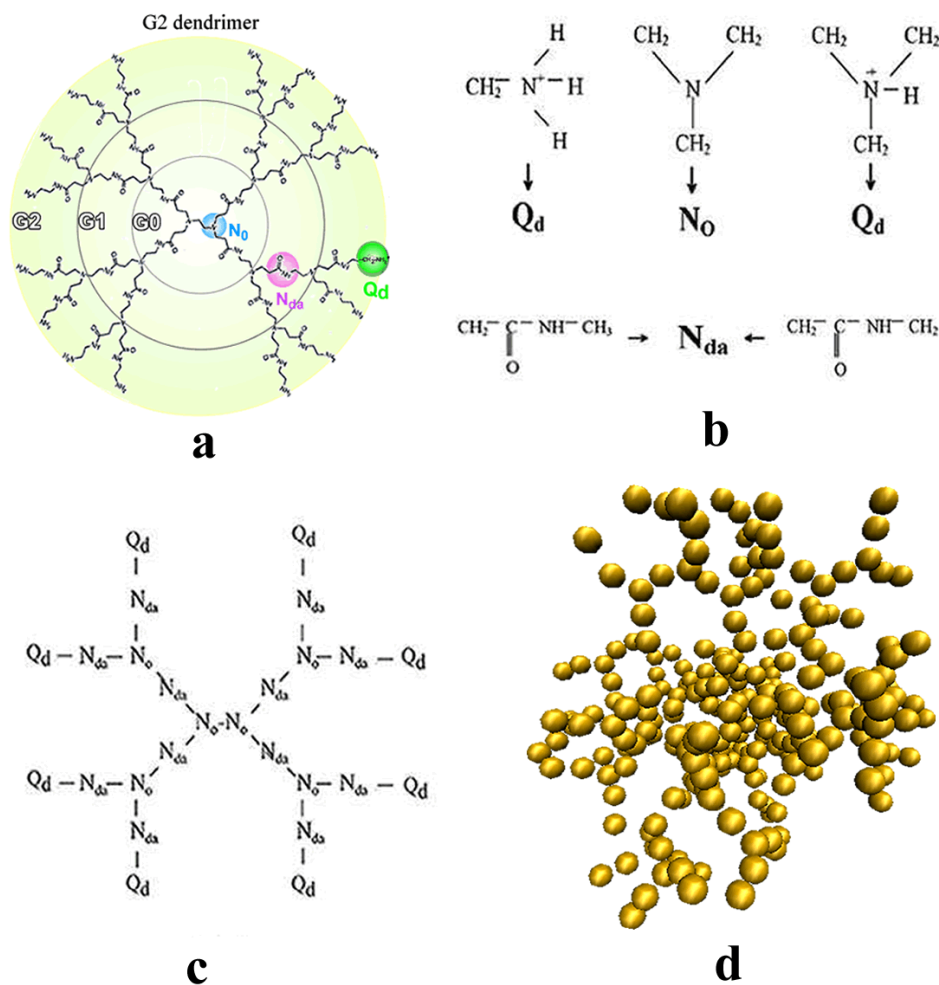


Figure S 2: (a) Mapping of the G2 polyamidoamine (PAMAM) dendrimer into the coarse-grained beads in the framework of MARTINI force field.^{2,3} (b) Mapping of dendrimer chemical moieties into coarse-grained beads. The dendrimer is composed of four different types of chemical moiety, each represented by a single bead type. N_0 stands for a neutrally charged group; Q_d represents a charged group with hydrogen-bond donors; N_{da} indicates a neutrally charged group with a hydrogen-bond donor and an acceptor. (c) Schematic illustration of the topology of the G1 PAMAM dendrimer with protonated terminals. The interior portion consists of N_0 and N_{da} moieties, respectively, for nodes and branches, and the surface consists of Q_d groups. Higher generations can be described by extending this topology. (d) The snapshot of the conformation of G4 dendrimers at low pH in our simulations, which consists of 250 CG beads in the framework of the MARTINI CG force field. The harmonic bonding and angle potentials are used to connect these beads.

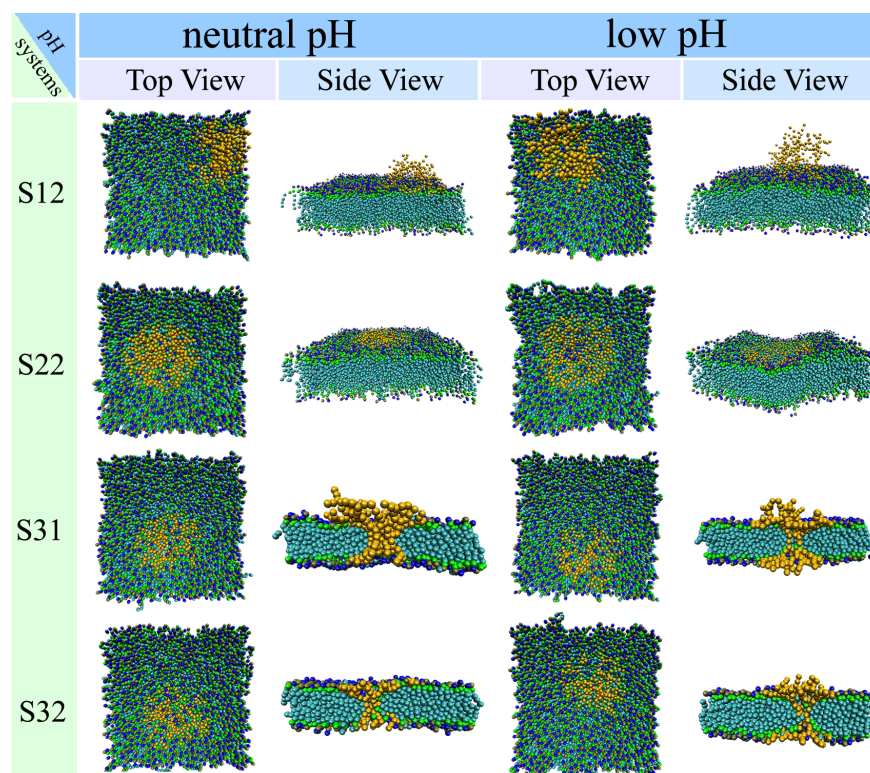


Figure S 3: Representative snapshots in equilibrated states of the G4 dendrimers interacting with lipid bilayers of other four subsystems (i.e., S12, S22, S31, and S32 of Table 1) in physiological and acidic pH environments. Orange beads represent G4 dendrimers, cyan beads represent tail groups of lipid bilayers, green and blue beads represent headgroups of the bilayers. Water and counterions are not shown for clarity. Compared with Figure 1 in the text, we find that the final conformation of dendrimer-bilayer complex of S12 subsystem is similar to that of S11 subsystem, that of S22 subsystem is similar to that of S21 subsystem, and these of S31 and S32 is similar to that of S33 subsystem. Thus, we only display the conformation of S11, S21, and S33 subsystems in the text. Orange beads represent G4 dendrimers, cyan beads represent tail groups of lipid bilayers, green and blue beads represent headgroups of the bilayers. Water and counterions are not shown for clarity.

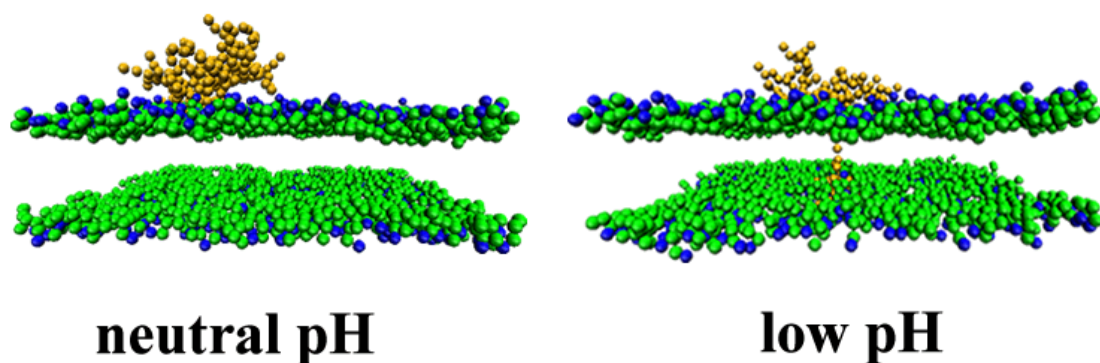


Figure S 4: The effect of electrostatic screen in the S33 subsystem at neutral and low pH values, where the final conformations are shown. We extend our investigation through adding 16 mM NaCl salt ions into the S33 subsystem, which provides an electrostatic screening effect. It can be seen that, in this case, the dendrimer just adheres on the membrane at neutral pH, while it penetrates into the bilayer at low pH. The result indirectly manifests the crucial role of electrostatic interactions in the dendrimer-membrane interactions. Orange beads represent G4 dendrimers, green and blue beads represent headgroups of the bilayers. Circles denote the position of pore. Water and counterions are not shown for clarity.

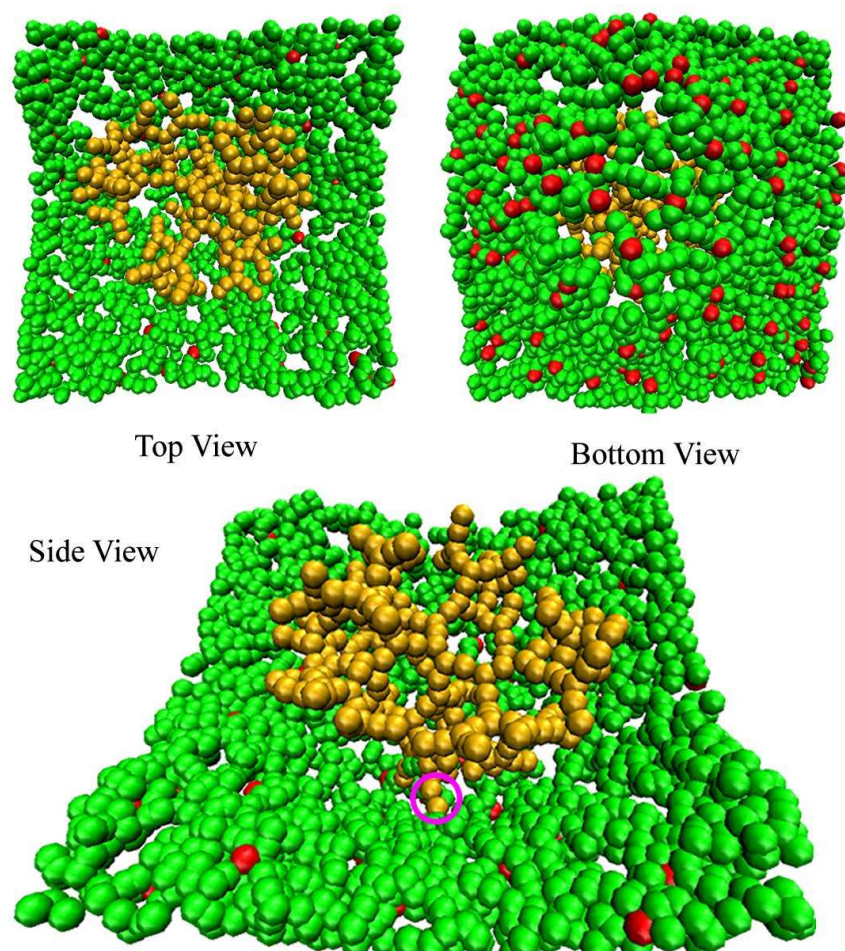


Figure S 5: Top, bottom, and side view of the 145 ns conformation of dendrimer-membrane complex of S33 system at low pH. The dendrimer leads to the sharp bending of asymmetric bilayer. At this time, the monomer of dendrimer firstly passes through the upper leaflet of bilayer and reach the downside of membrane. Orange beads represent G4 dendrimers, green beads represent headgroups of the bilayers except the headgroups of DPPS lipids which were denoted by red beads. Circles denote the position of the first monomer of dendrimer that arrives at the bottom leaflet of bilayer. Water and counterions are not shown for clarity.

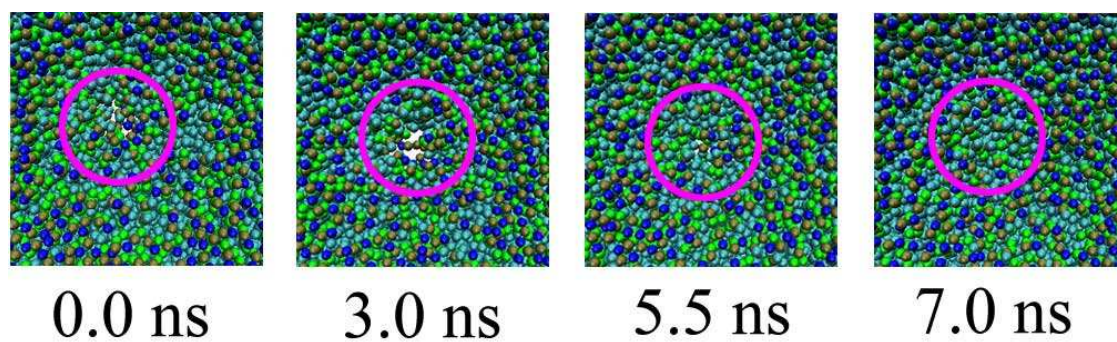


Figure S 6: Dynamics of pore vanishing in the tensionless membrane of S33 subsystem after the dendrimer was removed. cyan beads represent tail groups of lipid bilayers, green and blue beads represent headgroups of the bilayers. Circles denote the position of pore. Water and counterions are not shown for clarity.

- ¹ S. J. Marrink, A. H. de Vries, A. E. Mark, *J. Phys. Chem. B*, 2004, **108**, 750.
- ² L. Monticelli, S. K. Kandasamy, X. Periole, R. G. Larson, D. P. Tieleman, S. J. Marrink, *J. Chem. Theory and Comput.*, 2008, **4**, 819.
- ³ H. Lee, R. G. Larson, *J. Phys. Chem. B*, 2006, **110**, 18204.
- ⁴ R. H. Garrett, C. M. Grisham, *Biochemistry*, Tomson Brooks/Cole: Davis Drive, 2005.
- ⁵ F. Vögtle, G. Richardt, N. Werner, *Dendrimer Chemistry: Concepts, Syntheses, Properties, Applications*, Wiley-VCH: Verlag GmbH, 2009.
- ⁶ D. Cakara, J. Kleimann, M. Borkovec, *Macromolecules*, 2003, **36**, 4201.
- ⁷ P. K. Maiti, T. çağın, S. T. Lin, W. A. Giddard III, *Macromolecules*, 2005, **38**, 979.
- ⁸ I. Lee, B. D. Athey, A. W. Wetzel, et al. *Macromolecules*, 2002, **35**, 4510.
- ⁹ D. Van Der Spoel, E. Lindahl, B. Hess, G. Groenhof, A. E. Mark, H. J. C. Berendsen, *J. Comput. Chem.*, 2005, **26**, 1701.
- ¹⁰ H. J. C. Berendsen, J. P. M. Postma, W. F. Van Gunsteren, A. Dinola, J. R. Haak, *J. Chem. Phys.*, 1984, **81**, 3684.
- ¹¹ U. L. Essmann, L. Perera, M. L. Berkowitz, T. Darden, H. Lee, L. G. Pedersen, *J. Chem. Phys.*, 1995, **103**, 8577.
- ¹² W. Humphrey, A. Dalke, K. Schulten, *J. Mol. Graphics*, 1996, **14**, 33.